

# Final Report on the Project Nr. 13-360: New Detection Technique for Fault Tolerant Individual Pitch Control of Wind Turbines

## Abstract

Detection of the blade root moment sensor failures is an important problem for fault tolerant individual pitch control, which plays a key role in reduction of uneven blade loads of large wind turbines. A new method for detection of the blade root moment sensor failures which is based on variations induced by a vertical wind shear is described in this report. The detection is associated with monitoring of statistical properties of the difference between amplitudes of the first harmonic of the blade load, which is calculated in two different ways. The first method is based on processing of the load sensor signal, which contains a number of harmonics. The first harmonic is recovered via least squares estimation of the blade load signal with harmonic regressor and SDD (Strictly Diagonally Dominant) information matrix. The second method is a model-based method of estimation of the first harmonic, which relies on the blade load model and upwind speed measurements provided by multibeam LIDAR. This is a new application for future LIDAR-enabled wind turbine technologies. Moreover, adaptation of the load model in a uniform wind field is proposed. This adaptation improves accuracy of the load estimation and hence the performance of the blade load sensor failure detection method.

*Keywords:* Blade Root Moment Sensor Failure Detection, Fault Tolerant Individual Pitch Control, Estimation of the First Harmonic, Strictly Diagonally Dominant Matrix, Adaptation of Load Model, Multibeam LIDAR

# 1 Motivation and Description of the Detection Method

## 1.1 Individual Pitch Control and Unreliable Blade Load Measurements

IPC (Individual Pitch Control) is the only suitable tool for mitigation of uneven blade loads [1] - [9]. IPC reduces maintenance costs and increases efficiency and lifetime of the turbine components through significant contribution to the load reduction. IPC is based on the blade load measurements provided by strain gauge resistors, where the resistance changes in the case of loading. The lifetime of the strain gauge is normally not very long and the main sources of the errors are the following: (1) sensitivity to the temperature variations which results in a zero load drift, temperature distribution over the material and thermal stresses ; (2) transverse sensitivity ; (3) humidity which results in variation in stiffness of the composite materials ; (4) strain cycling which introduces a zero shift ; (5) fatigue of the material which results in a zero shift, change in gauge factor, and possible gauge failure in fatigue ; (6) cable effects that might change the resistance, capacitance, insulation, and screening.

The factors listed above together with many other factors is the reason for high failure rates of blade load sensors. The failure rates are especially high for off-shore wind turbines due to severe environmental conditions. An average failure rate is one failure per year. For wind turbines with three blades, the failure rate is approximately three failures per year [10].

Performance improvement of the blade load sensor failure detection mechanism is a challenge in the IPC system, which plays a key role in reduction of uneven blade loads of large wind turbines. On the other hand, new laser sensor (LIDAR) technologies which are capable of measuring wind speed at a distance in front of the turbine will be widely used in the future in a number of turbine control loops aiming to performance improvement via integration of proactive capabilities. This will result in LIDAR-assisted proactive turbine speed control, collective pitch angle control as well as yaw and individual pitch control, see [11] - [14] for details. Preview information, provided by the LIDAR usually results in a feedforward part which is properly integrated into the existing feedback controller. Information provided by the LIDAR might also be used for fault detection purposes (so far it was used for control only). LIDAR sensors are traditionally configured with a single beam. New generation of LIDAR sensors are equipped with many beams at different angles providing new opportunities for accurate estimation of incoming wind field [15],[16]. In particular, LIDAR-enabled blade load estimation may result in a new class of blade load fault detection methods with improved detection capabilities. This is a new application for future wind turbine technologies based on multibeam LIDAR.

Notice that the load model driven by upwind speed measurements is suitable for estimation of the first harmonic only, whereas load sensor signal contains a number of harmonics. Therefore a reduction of uneven loads is more efficient for IPC, which is driven by the load sensor signal,

provided that a pitch actuator is fast enough to counteract higher harmonics [8]. IPC which is based on LIDAR measurements [9] is used in the system in the case of blade load sensor failure. Information provided by LIDAR ensures fault tolerance of IPC as an ability of the system to maintain control objectives, despite the occurrence of a failure in the blade root moment sensor.

## 1.2 Detection Method Based on Turbine Cycle Variations

A new method for detection of the blade root moment sensor failures which is based on a vertical wind shear estimation is described in this report. Wind shear is almost always present in the wind speed distribution, see Figure 2 in [9], which illustrates a vertical wind shear. Traditional detection methods are usually based on monitoring of a change in mean value of the sensor signal (see [10] for example), whereas turbine cycle variations act as a disturbance, leading to deterioration of the detection performance and misdetection. This detection method is based on monitoring of the turbine cycle variations and captures information, which was previously ignored. Assessment of turbine cycle variations provides the basis for fast detection methods with respect to the methods, which are based on monitoring of the mean value. Fast detection is especially efficient in the case of drifting sensor failures.

The method is based on monitoring of the evolution of the first harmonic of the signal in the turbine cycle loading, which appears due to the wind shear. Amplitude of the first harmonic is estimated in two ways, which are described as follows:

(1) The first harmonic can be extracted from the blade root moment sensor signal, which contains a number of harmonics and a measurement noise. A number of algorithms can be used for estimation of the first harmonic, taking into account a property of persistence of excitation of the blade root moment sensor signal in the presence of the wind shear. This method is associated with processing of the blade load signal using least-squares algorithm with harmonic regressor [17] - [21] for estimation of amplitude of the first harmonic.

(2) LIDAR-enabled blade load estimation opens new opportunities for the model-based blade load sensor fault detection. The first harmonic of the turbine cycle loading can be estimated using upwind speed measurements in multibeam configuration which is illustrated in Figure 1. This method is referred as a model-based blade load estimation method, driven by upwind speed measurements. Estimation of the first harmonic described above is based on two sensors with different measurement principles, and therefore can be combined for a high performance failure detection. The detection is associated with monitoring of statistical properties of the difference between amplitudes of the first harmonic calculated in two different ways.

Notice that load sensors (strain gauges), located on the fixed part of the nacelle, which measure tilt and yaw nacelle moments, could also be used for estimation of the blade loads via inverse Coleman

transformation as it is described in [10]. The same measurement principle associated with estimated and measured blade loads together with inaccuracies in Coleman transformation (see [22] for details) result in poor detection performance in this case.

The fault detection method proposed in this report is associated with a change detection, where the change in parameters of distribution of the difference between amplitudes of the first harmonic identifies the fault.

Three types of faults can be detected: (1) abrupt jump faults with a step-like behavior, where the signal changes abruptly from the nominal value to a faulty value ; (2) incipient faults with a drift-like behavior, where the signal gradually changes from the nominal value to a faulty value ; (3) intermittent faults, where the signal changes from the nominal value to a faulty value, and returns to the nominal value after some time.

All three types of the faults can be identified via detection of the changes in the parameters of distribution of the difference between the amplitudes.

Notice that this report does not cover all types of faults which may appear in wind turbine. Additional fault scenarios together with a benchmark wind turbine model are presented in [23].

## 2 New Detection Method of the Blade Load Sensor Failures

### 2.1 Model of the Flapwise Bending Moment: Accounting for Higher Harmonics

Two wind speeds, measured at different heights, see Figure 1, is the input to the turbine load model. The periodic individual blade wind speeds  $V_i$ ,  $i = 1, 2, 3$ , defined at the center of each blade in rotating frame can be calculated using these two wind speeds (as boundary conditions), which together with the turbine rotor speed  $\omega_r$  are associated with the individual blade tip-speed ratio  $\lambda_i$  as follows:

$$\lambda_i = \frac{\omega_r R}{V_i} \quad (1)$$

where  $R$  is the rotor radius. Individual blade wind speeds have a fundamental frequency associated with a turbine rotational speed. The individual blade wind speed together with the pitch angle and rotor speed define the individual blade flapwise bending moment  $M_{f,i}$ , which can be presented as

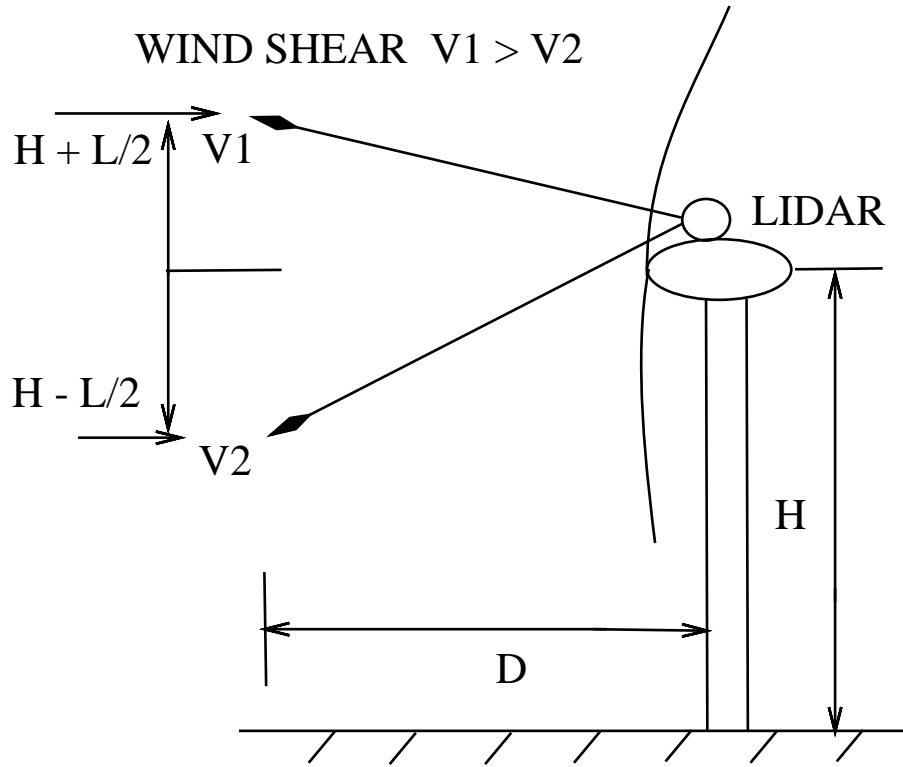


FIG 1: Multibeam LIDAR measurements of two wind speeds  $V_1$  and  $V_2$  (located at the heights which are equal to the hub height  $H$  with the half of the blade length  $\frac{L}{2}$  added/subtracted) at a distance  $D$  in front of the turbine. A periodic loading appears on the blades with the rotation of the turbine rotor in the presence of a vertical wind shear, which is associated with a change (increase) in wind speed with height,  $V_1 > V_2$ . This periodic loading has a number of harmonics and a first harmonic is associated with the frequency of the wind turbine rotational speed.

an average value and a periodic component induced by wind shear. This component contains the first harmonic of the turbine rotational frequency and high order harmonics and can be described as follows:

$$M_{f,i} = A_0 + \sum_{h=1}^d A_{h,i} \cos(h\omega_r t) \quad (2)$$

where  $A_0 = A_0(V, \omega_r, \beta_c)$  is the average value of the flapwise bending moment, and  $A_{h,i} = A_{h,i}(V_1, V_2, \omega_r, \beta_c)$  is the amplitude of the harmonic  $h$ , where  $d$  is a total number of harmonics. The average value of the flapwise bending moment depends on the hub wind speed  $V$ , turbine speed  $\omega_r$  and collective pitch angle  $\beta_c$ . The amplitudes depend on two winds speeds  $V_1$  and  $V_2$ , which characterize wind shear, see Figure 1, turbine speed and collective pitch angle.

Notice that wind shear consists of vertical and horizontal components. A vertical component is accounted only in this model as the most pronounced component of the wind shear. A horizontal component, which is not accounted in this model is treated as stochastic variations of the amplitudes.

## 2.2 Processing of Persistently Exciting Blade Root Moment Sensor Signal: Amplitude Estimation

Discrete-time measurements of individual blade flapwise bending moment  $M_{fk}$  (where index  $i$  is dropped for simplicity) with  $d$  harmonics can be written as follows:

$$M_{fk} = \sum_{h=1}^d A_{hk} \cos(h\omega_{rk}k) + \xi_k = \varphi_k^T \theta_{*k} + \xi_k \quad (3)$$

where  $\varphi_k$  is the harmonic regressor and  $\theta_{*k}$  is the vector of unknown parameters defined as follows:

$$\varphi_k^T = [\cos(\omega_{rk}k) \quad \cos(2\omega_{rk}k) \quad \cos(3\omega_{rk}k) \quad \dots \quad \cos(d\omega_{rk}k)] \quad (4)$$

$$\theta_{*k}^T = [A_{1k} \quad A_{2k} \quad A_{3k} \quad \dots \quad A_{dk}] \quad (5)$$

where  $\omega_{rk}$  is a discretized turbine speed,  $\xi_k$  is a zero mean white Gaussian measurement noise,  $k = 1, 2, \dots$  is the step number. Notice that the average value of the flapwise bending moment can be easily estimated using a low pass filter and subtracted from the individual blade flapwise bending moment signals. Therefore the signal (3) contains the periodic component only. Least-squares estimate

$$\theta_k^T = [\hat{A}_{1k} \quad \hat{A}_{2k} \quad \hat{A}_{3k} \quad \dots \quad \hat{A}_{dk}] \quad (6)$$

of unknown parameter  $\theta_*$  in a window of a size  $N$ , which is moving in time, can be written as follows [19]:

$$\theta_k = \left[ \sum_{j=k-N+1}^k \varphi_j \varphi_j^T \right]^{-1} \sum_{j=k-N+1}^k \varphi_j M_{fj} \quad (7)$$

and the first harmonic  $M_{ffk}$  is recovered according to the relation:

$$M_{ffk} = \hat{A}_{1k} \cos(\omega_{rk}k) \quad (8)$$

where  $\hat{A}_{1k}$  is estimated amplitude of the first harmonic.

The matrix  $\sum_{j=k-N+1}^k \varphi_j \varphi_j^T$  is called as information matrix and it is an SDD matrix for a sufficiently large window size [20]. SDD matrix can easily be inverted making algorithm computationally efficient and implementable. Moreover, estimated parameters can also be rapidly and accurately calculated without matrix inversion [21].

Estimation problem stated above is a challenging estimation problem due to time varying amplitudes and rotational speed. The accuracy of estimation can be improved via reduction of the window size for fast varying parameters. The properties of the information matrix based on harmonic regressor have not been studied for a sufficiently small window size  $N$ . The case, where the window size is not large enough for information matrix to be an SDD matrix is considered in Appendix. A positive definiteness of the information matrix based on harmonic regressor with four components is shown in this Appendix using partitioning method.

A measurement noise together with non-stationary nature of estimated parameters and turbine rotational speed are the main obstacles to high performance estimation of the first harmonic of the flapwise bending moment in real-time. Post-processing estimation, where all the signals are saved in the buffer and future values of the measured signal are available shows significant improvement with respect to real-time estimation, see Figure 2.

### 2.3 Model-Based Estimation of the Amplitude of the First Harmonic

Two wind speeds which are measured at a distance in front of the turbine (see Figure 1) are used for model-based estimation of the amplitude of the first harmonic of blade load. The wind speeds which are expected to arrive to the turbine site after some time can be calculated using a classical frozen turbulence assumption [24]. Expected periodic individual blade wind speeds  $V_{ie}$ ,  $i = 1, 2, 3$  defined at the center of each blade in rotating frame can be calculated using two expected wind speeds. Expected periodic individual blade wind speeds together with turbine speed and pitch angle

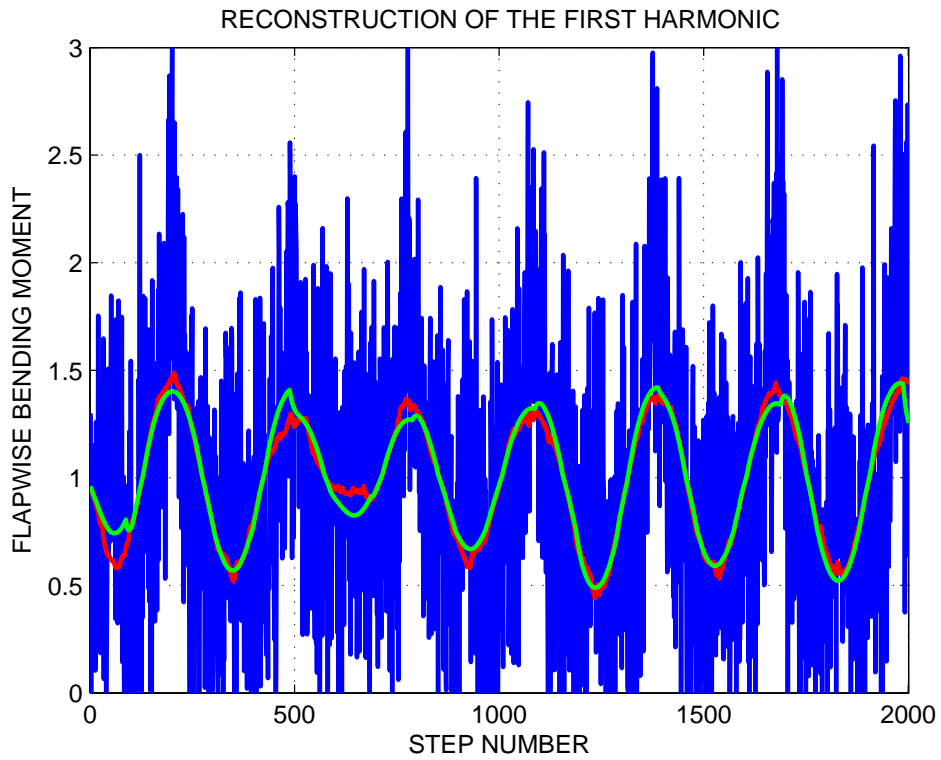


FIG 2: Reconstruction of the first harmonic from a noisy blade load signal in post processing. Measured signal of the flapwise bending moment, which contains four harmonics is plotted with a blue line. The first harmonic is plotted with a green line, and estimate of this harmonic is plotted with a red line. The flapwise bending moment is presented in normalized unit.

are the inputs to the look-up table, which estimate individual blade flapwise bending moments as follows:

$$M_{fm,i} = f(V_{ie}, \omega_r, \beta_c) \quad (9)$$

This model is suitable for estimation of first harmonic of turbine rotational frequency only. This harmonic appears in the load in the presence of the wind shear. Amplitude of this harmonic  $\hat{A}_{1mk}$  is estimated using least squares method.

Notice that two techniques of estimation of the first harmonic described above are based on sensors with different measurement principles and therefore can be combined for high performance failure detection.

## 2.4 Monitoring of the Amplitude of the First Harmonic: Outlier Detection

Blade load sensor failure detection mechanism is driven by two sensors: (1) LIDAR, which measures two wind speeds at a distance in front of the turbine, and (2) blade strain gauges, which measure a flapwise bending moment. A chart of the detection mechanism is presented in Figure 3. Two amplitudes of the first harmonic of rotational frequency are estimated and compared. A difference between the amplitudes  $\Delta A_k = \hat{A}_{1mk} - \hat{A}_{1k}$ , which is calculated in two ways is normally distributed with a zero mean value for healthy system. The parameters of such distribution can be identified using a sufficiently large number of measured points in the case of healthy system. The fault detection is associated with a change detection, where the change of the parameters of this distribution identifies the fault.

A slow drift of the amplitude of the first harmonic of the strain gauge signal is shown as an example in Figure 4 with corresponding distributions plotted in Figure 5. Such a drift may appear due to the fatigue of the material in the cycle loading or humidity change, which results in a change of gauge factor, see Section 1.1 for all types of the faults.

Each sample of the difference between amplitudes should belong to a parent distribution, associated with healthy system. The fault is detected, if the sample is identified as an outlier<sup>1</sup>. An outlier is detected via *Two Sample t-Test*, where a hypothesis that a mean value of the distribution that describes healthy system is equal to suspected outlier, which is treated as a mean value of a virtual distribution [25], is taken as a null hypothesis. This hypothesis is tested against alternative hypothesis that the observation point does not belong to parent distribution, that describes healthy system. The failure is detected, if the null hypothesis is rejected in favor of alternative hypothesis. A slow drift can also be detected via monitoring of the fluctuations of the mean value of the difference between the amplitudes. This monitoring is performed in a window of a certain size, which

---

<sup>1</sup>outlier is an observation point, which is distant from other observations

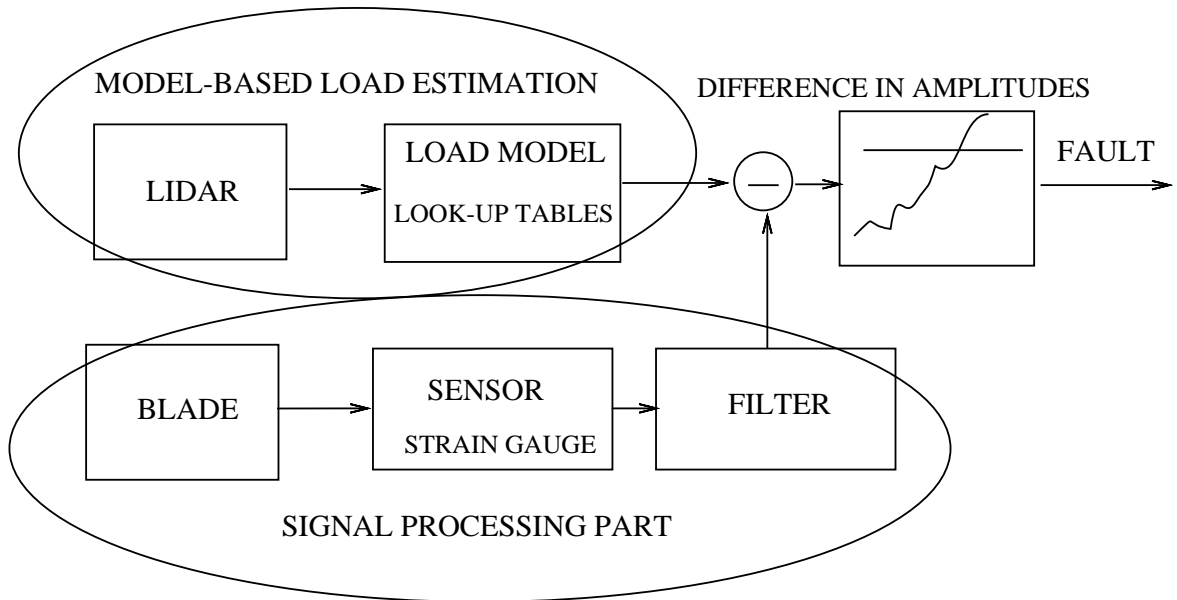


FIG 3: Detection of the blade load sensor faults.

is moving in time. Notice that the difference in mean values should be statistically significant for reliable detection of the fault. This can be verified using *Two Sample t-Test*, where a significance level represents trade-off between the fastness and detection performance.

### 3 Adaptation of the Load Model

The performance of the detection mechanism, described above depends on the performance of the load model, which is a mean value model that describes the flapwise blade root bending moment, see Figure 3. The model of the flapwise bending moment is presented in the form of look-up tables (the surfaces in three dimensional space) with the tip-speed ratio and blade pitch angle as input variables. The mean value of the bending moment calculated via look-up tables should coincide

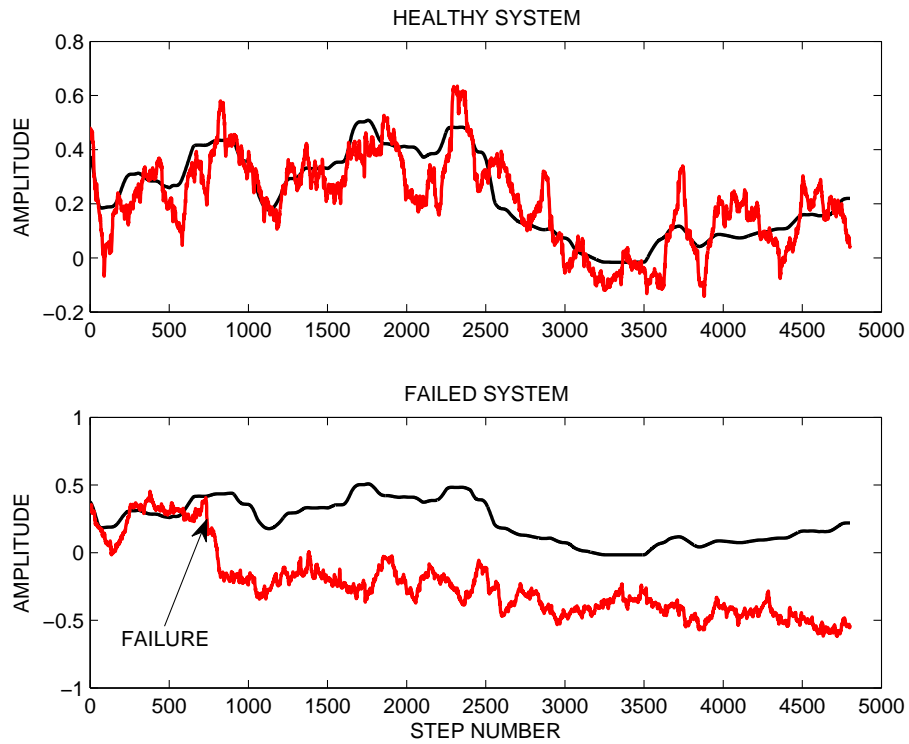


FIG 4: A time chart of the amplitudes of the first harmonic of healthy system (the first subplot), and failed system (the second subplot). Amplitudes of the first harmonic calculated using load model and sensor signal are plotted with black and red lines respectively. Incipient fault associated with a slow drift occurs in the step number 700. Histograms of healthy and failed systems are plotted in Figure 5.

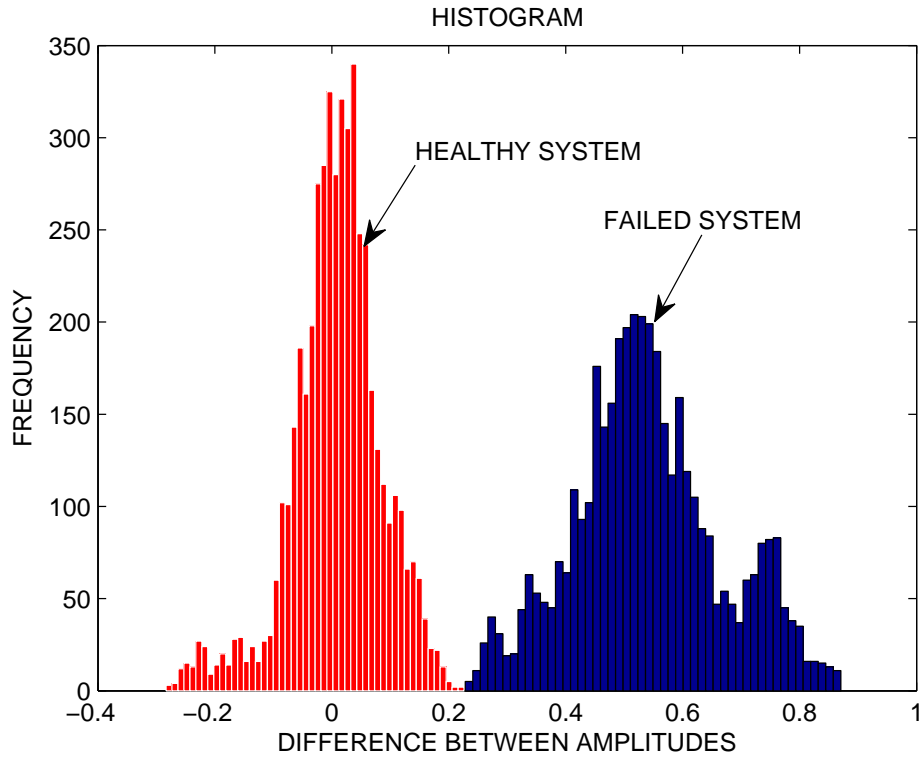


FIG 5: Histogram of the difference between the amplitudes of first harmonic for healthy system (plotted with red color) and for failed system, plotted with blue color.

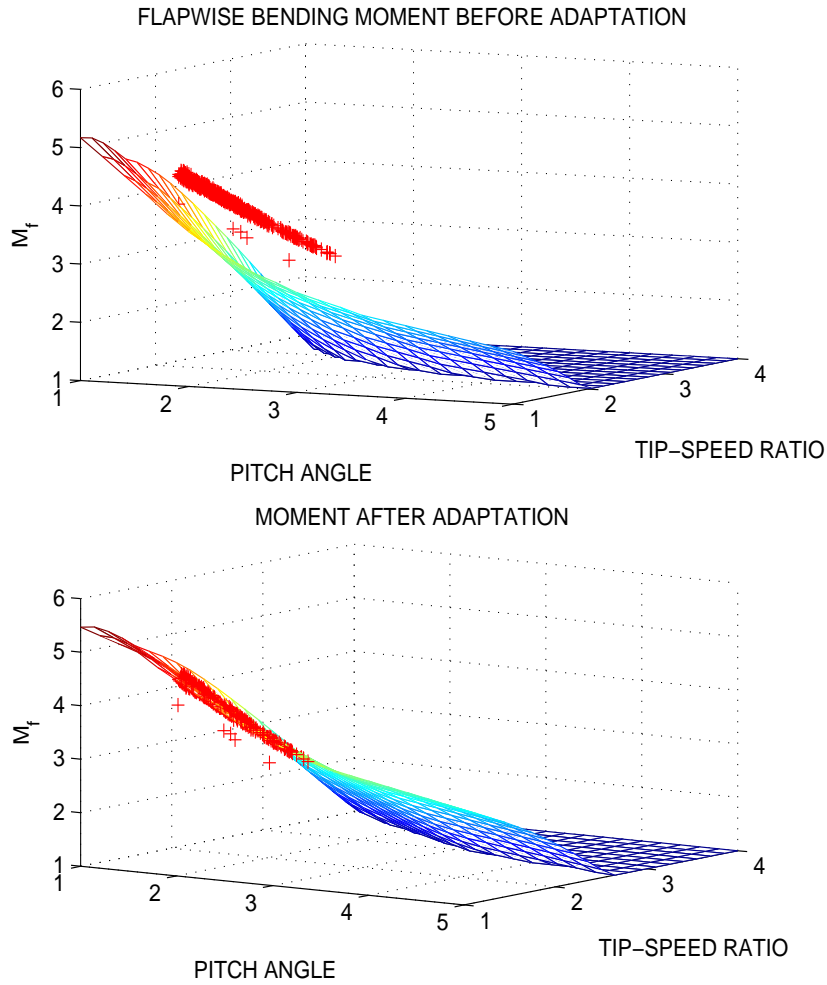


FIG 6: The flapwise bending moment is presented as a surface with tip-speed ratio and pitch angle as input variables for a certain turbine speed [14]. Mean values of measured flapwise bending moment are plotted with plus signs of a red color. The surface is adapted against measured data, minimizing deviations between the surface and measured points. All the variables are presented in normalized units.

with the outputs of the blade load sensors in a uniform wind field for healthy system. Deviations between the load sensor measurements and output of the model necessitate adaptation of the model, provided that the wind field is uniform. The uniformity of the wind speed across the rotor swept area is detected by comparison of the blade load sensor signals of all three blades and/or by LIDAR measurements. Average values of the load calculated using blade load sensors in a number of working points are memorized for adaptation of look-up tables. The data should be acquired over a relatively large time segment to ensure statistical consistency. Notice that additional requirements may be imposed on input data to avoid erroneous adaptation. If new data is available in a certain operating region only (for example at low wind speeds and for small pitch angles), then the part of the surface parameters is adapted (for example gradient in pitch angle direction). Adaptation of the look-up table is associated with a motion of the surface in three dimensional space, see Figure 6. The position and the orientation of the surface in three dimensional space change only after adaptation, which in turn, allows for a prediction of the bending moment for a wide range of operating variables. This adaptation method was developed first in automotive applications [25] and was successfully applied to turbine model validation with fusion of simulation and measurement data on Big Glenn wind turbine, located outside Gothenburg, Sweden [26].

## 4 Conclusion

Increasing demands on operational reliability, safety and power output of wind turbines necessitate the development of new high performance fault detection techniques. High performance fault detection is directly associated with predictive maintenance [27], where a component is replaced before the system breaks down, which implies significant savings as well as increases power output. Moreover, high performance fault detection methods are the basis for novel fault tolerant turbine control strategies, where a fault is predictively detected, and the turbine is switched to a safe operation mode to prevent damages, until a maintenance crew arrives to the turbine site. This extends the turbine operation time and increases the power output. Fault tolerance is associated with an ability of the turbine control system to maintain control objectives, despite the occurrence of a fault [28] - [30]. New blade load sensor fault detection technique proposed in this report is the basis for high performance fault tolerant IPC. This is also a new application for future multibeam LIDAR technology, which is utilized now in the preview based control only. New detection algorithms can be easily integrated into existing IPC functionality aiming for improvement of uneven load reduction for large turbines.

# Acknowledgement

The authors are grateful to WindVector AB and Albert Santiago from Avent Lidar Technology for interesting discussions about multibeam LIDAR technologies.

# References

- [1] Bossanyi E., Individual Blade Pitch Control for Load Reduction, *Wind energy*, N 6, 2003, pp. 119-128.
- [2] Larsen T., Madsen H. and Thomsen K. Active Load Reduction Using Individual Pitch, Based on Local Blade Flow Measurements, *Wind Energy*, N 8, 2005, pp. 67-80.
- [3] Stol K., Zhao W., and Wright A., Individual Blade Pitch Control for the Controls Advanced Research Turbine (CART), *Journal of Solar Energy Engineering*, vol. 128, November 2006, pp. 498-505.
- [4] Selvam K., Kanev S., van Wingerden J., van Engelen T. and Verhaegen M., Feedback-Feedforward Individual Pitch Control for Wind Turbine Load Reduction, *Int. J. Robust Non-linear Control*, vol. 19, 2009, pp. 72-91.
- [5] Lackner M. and van Kuik G., A Comparison of Smart Rotor Control Approaches Using Trailing Edge Flaps and Individual Pitch Control, *Wind Energy*, vol.13, 2010, pp. 117-134.
- [6] Jelavic M., Petrovic V., and Peric N., Estimation Based Individual Pitch Control of Wind Turbine, *Automatika: Journal for Control, Measurement, Electronics, Computing and Communications*, vol. 51, June 2010, pp. 181-192.
- [7] Bossanyi E., Fleming P., Wright A., Validation of Individual Pitch Control by Field Tests on Two- and Three-Bladed Wind Turbine, *IEEE Transactions on Control Systems Technology*, vol. 21, No. 4, 2013, pp. 1067-1078.
- [8] Petrovic V., Campagnolo F., Experimental Validation of Wind Turbine Higher Harmonic Control Using Shaft Loads Measurements, 2013 European Control Conference (ECC), July 17-19, 2013, Zurich, Switzerland, pp. 472-477.
- [9] Stotsky A. and Egardt B., Individual Pitch Control of Wind Turbines: Model-Based Approach, *Proc. IMechE Part I: Journal of Sytems and Control Engineering*, vol. 227, N 7, 2013, pp. 602-609.

- [10] Wei X., Verhaegen M., and van Engelen T., Sensor Fault Diagnosis of Wind Turbines for Fault Tolerant, Proceedings of the 17-th World Congress, The International Federation of Automatic Control, Seoul, Korea, July 6-11, 2008, pp. 3222-3227.
- [11] Johnson K., Pao L., Balas M., and Fingersh L, Control of Variable-Speed Wind Turbines: Standard and Adaptive Techniques for Maximizing Energy Capture, IEEE Control Systems Magazine, vol. 26, June 2006, pp. 70 - 81.
- [12] Laks J., Pao L., Wright A., Kelley N. and Jonkman B., The Use of Preview Wind Measurements for Blade Pitch Control, Mechatronics, 21, 2011, pp. 668-681.
- [13] Wang N., Johnson K. and Wright A., FX-RLS-Based Feedforward Control for LIDAR-Enabled Wind Turbine Load Mitigation, IEEE Transactions on Control Systems Technology, vol. 20, N 5, September 2012, pp. 1212-1222.
- [14] Stotsky A., Egardt B. and Carlson O., An Overview of Proactive Wind Turbine Control, Energy Science & Engineering, Wiley, N 1, 2013, pp. 1-10.
- [15] Wagenaar J., Davoust S., Medawar A., Coubard-Millet G. and Boorsma K., Turbine Performance Validation: The Application of Nacelle LIDAR, EWEA 2014, Barcelona, Spain, March 10 - 13, 2014.
- [16] Klasen L., Lidar Systems for Wind Energy Applications, Proceeding of Swedish Society of Automated Image Analysis, Symposium on Image Analysis, Luleå, March 11-12, 2014, pp 97-100.
- [17] Ioannou P. and Sun J., Robust Adaptive Control, Englewood Cliffs, NJ: Prentice-Hall, 1996.
- [18] Bayard D., A General Theory of Linear Time-Invariant Adaptive Feedforward Systems with Harmonic Regressors, IEEE Transactions on Automatic Control, vol. 45, No 11, 2000, pp. 1983-1996.
- [19] Ljung L., System Identification: Theory for the User, Upper Saddle River, NJ: Prentice-Hall, 1999.
- [20] Stotsky A. Recursive Trigonometric Interpolation Algorithms, Proceedings of the Institution of Mechanical Engineers, Part I: Journal of Systems and Control Engineering, vol. 224, No. 1, 2010, pp. 65-77.
- [21] Stotsky A., Robust Least-Squares Estimation with Harmonic Regressor: High Order Algorithms, 52-nd IEEE Conference on Decision and Control, December 10-13, 2013. Florence, Italy, pp. 6516-6521.

- [22] Bir G., Multiblade Coordinate Transformation and Its Application to Wind Turbine Analysis, Preprint NREL/CP-500-42553 January 2008.
- [23] Odgaard P. , Stoustrup J. and Kinnaert M., Fault-Tolerant Control of Wind Turbines: A Benchmark Model, IEEE Transactions on Control Systems Technology, vol. 21, No. 4, July 2013, pp. 1168 - 1182.
- [24] Taylor G., The Spectrum of Turbulence, Proc. R. Soc. Lond., vol. 164, 1938, pp. 476-490.
- [25] Stotsky A. Automotive Engines: Control, Estimation, Statistical Detection, Springer-Verlag, Berlin-Heidelberg, 2009, 215 pages.
- [26] Stotsky A., Wind Turbine Model Validation: Fusion of Simulation and Measurement Data, Proceedings of the Institution of Mechanical Engineers, Part I: Journal of Systems and Control Engineering, DOI: 10.1177/0959651814547442, August 2014.
- [27] Bertling L., Reliability Centred Maintenance for Electric Power Distribution Systems, Doctoral thesis KTH, 429 pages, Stockholm, Sweden, 2002, ISBN 91-7283-345-9.
- [28] Esbensen T., Sloth C., Fault Diagnosis and Fault-Tolerant Control of Wind Turbines, Technical Report, Faculty of Engineering, Science and Medicine, Department of Electronic Systems, Section for Automation and Control, Aalborg University, Denmark, 2009, 167 pages.
- [29] Pourmohammad S., Fekih A., Fault-Tolerant Control of Wind Turbine Systems - A Review, Proceeding of Green Technologies Conference (IEEE-Green), 2011 IEEE, Baton Rouge, LA, 14-15 April 2011, pp. 1-6.
- [30] Rezaei V. and Johnson K., Robust Fault Tolerant Pitch Control of Wind Turbines, 52-nd IEEE Conference on Decision and Control, December 10-13, 2013. Florence, Italy, pp. 391-396.
- [31] Horn R. and Johnson C. Matrix Analysis, Cambridge University Press, 1985.

## Appendix

### Positive Definiteness of Information Matrix for Insufficiently Large Window Size: Partitioning Method for the Case of Four Harmonics

Consider the following harmonic regressor:

$$\varphi_k^T = [\cos(\omega k) \quad \cos(2\omega k) \quad \cos(3\omega k) \quad \cos(4\omega k)] \quad (10)$$

where  $\omega$  is a constant rotational frequency and  $h\omega$  with  $h = 2, 3, 4$  are higher harmonics,  $k = 1, 2, \dots$  is the step number.

Consider the following information matrix calculated over the window of a size  $N$  :

$$G = G^T = \sum_{k=1}^N \varphi_k \varphi_k^T = \begin{bmatrix} g_{11} & g_{12} & g_{13} & g_{14} \\ g_{12} & g_{22} & g_{23} & g_{24} \\ g_{13} & g_{23} & g_{33} & g_{34} \\ g_{14} & g_{24} & g_{34} & g_{44} \end{bmatrix}$$

Elements of the matrix  $G$  can be evaluated explicitly using the following relation:

$$\sum_{k=1}^N \cos(h\omega k) = \frac{\cos\left(\frac{N+1}{2}h\omega\right) \sin\left(\frac{N}{2}h\omega\right)}{\sin\frac{h\omega}{2}} \quad (11)$$

where  $h = 1, \dots, 4$ . The first two elements of the first row of this matrix are presented below:

$$\begin{aligned} g_{11} &= \sum_{k=1}^N \cos^2(\omega k) = \underbrace{\frac{N}{2}}_{\text{average part}} \\ &+ \underbrace{\frac{\sin(N\omega) \cos((N+1)\omega)}{2 \sin \omega}}_{\text{periodic part}} \end{aligned} \quad (12)$$

$$\begin{aligned} g_{12} &= \sum_{k=1}^N \cos(\omega k) \cos(2\omega k) = \\ &= \frac{1}{2} \frac{\cos\left(\frac{3(N+1)}{2}\omega\right) \sin\left(\frac{3N}{2}\omega\right)}{\sin\frac{3\omega}{2}} \\ &+ \frac{1}{2} \frac{\cos\left(\frac{N+1}{2}\omega\right) \sin\left(\frac{N}{2}\omega\right)}{\sin\frac{\omega}{2}} \end{aligned} \quad (13)$$

All other elements of this matrix can be evaluated using similar arguments.

## 4.1 Partitioning of Matrix $G$

Symmetric matrix  $G$  can be partitioned as follows:

$$G = \begin{bmatrix} A & B \\ B^T & C \end{bmatrix}$$

where  $A = \begin{bmatrix} g_{11} & g_{12} \\ g_{21} & g_{22} \end{bmatrix}$ ,  $B = \begin{bmatrix} g_{13} & g_{14} \\ g_{23} & g_{24} \end{bmatrix}$  and

$C = \begin{bmatrix} g_{33} & g_{34} \\ g_{34} & g_{44} \end{bmatrix}$ . Notice that the diagonal elements of the matrices  $A$  and  $C$  have periodic part

and average part  $\frac{N}{2}$ , whereas all other elements of matrices  $A, B$  and  $C$  have periodic parts only.

Matrix  $G$  becomes an SDD matrix for a sufficiently large window size  $N$ . Suppose that the window size  $N$  is large enough for matrices  $A$  and  $C$  to be SDD matrices, but it is not sufficiently large for matrix  $G$  to be an SDD matrix. The matrix  $G$  is positive definite if and only if the matrices  $A$  and  $C - B^T A^{-1} B$  are positive definite matrices (see theorem 7.7.6 in [31]). Inverse of the matrix  $A$  can

be approximated as  $A^{-1} \approx D = \frac{2}{N} I$ , when neglecting periodic part in matrix  $A$ , where  $I$  is the identity matrix. The matrix  $B^T B$  also has an average part that is proportional to the window size  $N$ . This part is canceled by the diagonal elements of matrix  $D$  in the term  $B^T A^{-1} B$ . Therefore there exists a large enough window size  $N$  such that the matrix  $C - B^T A^{-1} B$  is an SDD matrix. Hence the matrix  $G$  is a positive definite matrix, since matrix  $A$  is also an SDD and positive definite matrix. Notice that the matrix  $G$  is not an SDD matrix.

This technique of determination of positive definiteness of information matrix is illustrated via numerical example in the next Section.

## Numerical Example

Consider the following information matrix  $G$  based on the regressor (10) with  $\omega = 0.0228$  and the window size  $N = 83$ :

$$G = \begin{bmatrix} 34.4747 & 16.2691 & -1.9465 & -4.8693 \\ 16.2691 & 46.5787 & 19.8127 & -10.6043 \\ -1.9465 & 19.8127 & 37.9209 & 22.3866 \\ -4.8693 & -10.6043 & 22.3866 & 42.5117 \end{bmatrix}$$

This matrix  $G$  is not an SDD matrix since the diagonal elements in the second and the third rows are not larger than the sum of the magnitudes of all the other (non-diagonal) entries in the

second and third rows. Nevertheless, the matrices  $A = \begin{bmatrix} 34.4747 & 16.2691 \\ 16.2691 & 46.5787 \end{bmatrix}$  and  $C - B^T A^{-1} B = \begin{bmatrix} 26.7629 & 26.5384 \\ 26.5384 & 40.0503 \end{bmatrix}$  are positive definite and SDD matrices. Therefore the matrix  $G$  is a positive definite matrix. Notice that the matrices  $A$  and  $C - B^T A^{-1} B$  are still positive definite (but not SDD) matrices even for a sufficiently small window size  $N$ .

## Publication Results of the Project

The following journal paper based on the results presented above was published :

Stotsky A., Blade Root Moment Sensor Failure Detection Based on Multibeam LIDAR for Fault-Tolerant Individual Pitch Control of Wind Turbines, *Energy Science & Engineering*, vol. 2, N 3, 2014, pp.107-115.

The following paper was accepted for presentation on the 2014 IEEE 53-rd Annual Conference on Decision and Control (CDC) to be held on the 15 - 17 of December, 2014 in J.W. Marriott Hotel Los Angeles, CA, USA :

Stotsky A., High Order Algorithms in Robust Least-Squares Estimation with SDD Information Matrix: Redesign, Simplification and Unification.

## Participants

Project Leader: Professor Ola Carlson  
Researcher: Docent Alexander Stotsky

Department of Energy & Environment, Division of Electric Power Engineering, Chalmers  
University of Technology, Gothenburg SE - 412 96, Sweden.  
Email: [alexander.stotsky@chalmers.se](mailto:alexander.stotsky@chalmers.se)